ROYAL AERONAUTICAL SOCIETY

RESEARCH ARTICLE

A sensitivity study of the transonic aerodynamics of a strut-braced airframe

P. Nagy ⬤, B. Jones ⬤, E. Minisci ⬤ and M. Fossati ⬤

Aerospace Centre, Department of Mechanical and Aerospace Engineering, University of Strathclyde, Glasgow, UK
Corresponding author: M. Fossati; Email: marco.fossati@strath.ac.uk

Abstract
The aerodynamic performance of an ultra-high aspect ratio strut-braced wing design is assessed for flight at cruise. The sensitivity of a selected airframe design from a recent CleanSky2 project to operating conditions around the design point is quantified using the adaptive-cut high-dimensional model representation (HDMR) method, which allows for the decomposition of the parameter space into smaller subdomains to isolate the parameter interactions and influence on the aerodynamic forces. A comparative analysis with a cantilever wing configuration is performed to identify the role of the strut on the sensitivity of the design. Insight into the transonic performance is gained by characterisation of buffet limits and drag rise. Results show that, for the selected optimised airframe configuration, small changes in freestream parameters can lead to significant reduction in performance due to drag divergence triggered by the shock wave generated at the strut-wing junction and at the fuselage-strut intersection. Cruise conditions can be achieved without buffet onset throughout much of the parameter space. Safety margins associated with buffeting are satisfied, but sensible limits are imposed on the flight envelope for this configuration.

Nomenclature

a_i	i^{th} POD coefficient
AR	aspect ratio
C_D	coefficient of drag
C_L	coefficient of lift
f_c	central value in the context of HDMR
$f(\mathbf{U})$	multivariate function of interest in the context of HDMR
F_i	Increment function of ith parameter in the context of HDMR
h	altitude
L/D	lift-to-drag ratio
M	Mach number
N	load factor
N_m	number of POD modes
N_u	number of parameters in the context of HDMR
v	velocity
Re/m	Reynolds number per unit metre
$\mathbf{u}$	exact solution in the context of ROM
$\hat{\mathbf{u}}$	approximate solution in the context of ROM
$\mathbf{x}$	location in parameter space in the context of ROM

Greek symbol

α	angle-of-attack
ϕ_i	i^{th} POD mode
σ	buffet onset criterion

Acronyms

AoA	angle-of-attack
CFD	computational fluid dynamics
CW	cantilever wing
dd-ROM	data-driven reduced order modelling
HDMR	high-dimensional model representation
HiFi	high fidelity
JST	Jameson-Schmidt-Turkel
POD	proper orthogonal decomposition
RANS	Reynolds-averaged Navier-Stokes
RBF	radial basis function
ROM	reduced order model
SA	Spalart-Allmaras
SBW	strut-braced wing
UHARW	ultra-high aspect ratio wing

1.0 Introduction

Next-generation non-conventional commercial aircraft are a critical area of research as they are considered the key to achieving emission goals and performance requirements in the coming decades. Ultra-high aspect ratio wings (UHARW) are a promising design choice to achieve these goals [1] due to the advancement of pre-requisite technologies that will enable these designs as well as advances in computational methods and capacity that perform complex, often multi-disciplinary design and optimisation, which is required for next-generation configurations. The high aspect ratio and larger wing span offers reduction in induced drag, thus better lift-to-drag ratio, L/D. However, large wing span leads to higher wing loading, and aeroelasticity becomes a dominant aspect of the design. To mitigate adverse effects on the structural efficiency due to the increased loads on the wing, the concept of truss- or strut-bracing has been introduced. The reinforcement provided by strut-braced wings (SBWs) can in fact surpass the structural efficiency of conventional configurations and allow for thinner wing sections [2]. As these aircraft fly in the transonic regime, thinner aerofoils prove to be advantageous in reducing or eliminating wave drag. As a direct consequence of this, a lower sweep angle becomes possible, which in turn can lead to further improvement in the aerodynamic efficiency due to larger extension of laminar flow and indeed promote the use of technologies such as natural laminar flow aerofoils [3].

The well-known SUGAR airframe [4] has provided an extensive platform for research of SBWs as well as resulting in the announcement of the Boeing X-66 full-scale flight demonstrator. Another example is ONERA's ALBATROS project [5] which aimed to evaluate the potential performance gains offered by the SBW configuration by decoupled aerodynamic and structural parametric studies. Recently concluded European projects realised within the CleanSky2 Joint Undertaking programme, namely RHEA and U-HARWARD, also focused on the development of SBW designs. Performance gains in terms of L/D have conservative estimates of around 13%, and up to 50% improvement promised by more radical designs [6–8].

The aerodynamics of the wing-strut junction and aerodynamic optimisation to alleviate adverse effects arising from such geometry has been the focus of several works. Ko et al. [7] identify the nozzle (or channeling) effect to be a dominant feature in the region of the wing-strut junction, contributing to a large spanwise extension of the shock wave on the strut. They found that the pylon itself has little role

in the interference effects. They mitigate the shock formation by flattening the suction side of the strut near the junction, leading to negative local lift. Note however that such reduction of the strut thickness may introduce significant problems for the structure. In a more recent work, Chau and Zingg [6] performed aerodynamic optimisation on a regional transonic SBW design, wherein the shock formation and separation at the wing-strut and strut-fuselage junctions were almost completely eliminated by locally deforming the geometry. For example, at the wing-strut junction the strut is twisted to provide negative lift, which is offset by a locally optimised wing shape. Moreover, the aerofoils near the junction are shaped to mitigate the acceleration of flow brought on by channeling. Similar shape deformation was achieved through aerodynamic optimisation by Secco and Martins [9]. They highlight the importance of optimising the strut shape, rather than the wing shape to achieve efficient drag reduction.

Parametric studies and multidisciplinary design and optimisation (MDO) studies are conducted primarily at a conceptual design level. Some effort is directed towards the comparative assessment of cantilever, strut- and truss-braced designs via MDO methodology, e.g. works done by Gur et al. [10] and Seber et al. [11]. Both studies indicate truss-braced designs as favourable to SBW, albeit the effect of the inherently more complex geometry on the aerodynamic environment cannot be assessed due to the limitations of the low-fidelity tools. An MDO study is conducted by Sohst et al. [12] where Reynolds-averaged Navier-Stokes (RANS) solutions are used to improve the drag prediction of lower-order methods. Chakraborty et al. [13] conducted a global sensitivity study to compare various strut- and truss-braced geometries. In addition, another novel configuration, the morphing-wing concept is assessed by Gong and Ma [14] through a variance-based sensitivity analysis method based on Euler solutions and corrections for viscous effects, presenting a higher-fidelity approach than other studies.

As discussed above, high-fidelity methods are used primarily in the context of aerodynamic shape optimisation rather than parametric studies or design space explorations, which usually favour lower-order methods. In this work, a high-fidelity-based sensitivity analysis is performed to assess the design robustness of a selected UHAR-SBW airframe design from U-HARWARD as well as characterise its behaviour near cruise conditions, with special care taken to assess transonic aerodynamic phenomena. The knowledge gained from the high-fidelity data presented in this work may be leveraged by future design efforts involving similar SBW configurations, noting that publicly available high-fidelity data for similar transonic transports is still relatively limited. Furthermore, the methodology adopted in this work has the flexibility to be applied in other contexts. For example, in a preliminary design setting, it enables the identification of a *good* baseline geometry and nominal operating conditions in a computationally efficient manner, which can then serve as a starting point for a more complex MDO study.

The adaptive-cut high dimensional model representation (A-cut HDMR) method is used to evaluate the sensitivity of the aircraft to operating conditions. The study is based on high-fidelity computational fluid dynamics (CFD) computations, and supported using a data-driven reduced order modelling (dd-ROM) approach to alleviate the high computational expense. A methodology combining an aerodynamic dd-ROM with A-cut HDMR has been introduced by the authors [15] in a recent study of another UHAR-SBW airframe.

This work is organised as follows: Section 2 gives a brief outline of the sensitivity analysis approach, then Section 3 details the aerodynamic test case, specifically the numerical setup and the SBW geometry. Section 4 presents the results of the sensitivity study, while Section 5 shows a comparative analysis with a cantilever wing configuration in an effort to quantify the influence of the strut. Transonic drag rise and buffeting of the aircraft are assessed separately, the results of the analysis are presented in Section 6. Section 7 presents the concluding remarks.

2.0 Sensitivity analysis approach

To perform the sensitivity analysis, the response of the function of interest is decomposed into individual parameter contributions and their interactions. This allows to quantify the influence as well as rank the importance of each contribution. The function response of each contribution also allows to gain insight

into the physics of the behaviour. The A-cut-HDMR approach is used to realise the decomposition, using C_L and C_D data primarily from RANS simulations. Computations are done on the 3D airframe geometry, and the aerodynamic loads on the surface are integrated to obtain C_L and C_D. Then the domain decomposition is driven by a set of these aerodynamic coefficients. If the adaptive process requires new points, additional CFD is computed and C_L, C_D values are then extracted. Since for the lowest ranked interaction the adaptive sampling of the HDMR queries too many CFD points thus leading to significantly increased computational costs, a proper orthogonal decomposition (POD)-based dd-ROM approach is adopted – in a sense substituting CFD – that allows uncovering said low ranking interactions in a computationally efficient manner.

In the following subsections a brief description is given for the A-cut HDMR and the dd-ROM methods. For a more detailed description please refer to the authors' previous paper [15] where the methodology was introduced for a similar aerodynamics application.

2.1 Adaptive-cut high dimensional model representation method

The A-cut-HDMR [16–18] is a probabilistic non-intrusive method, which is used to seek a decomposition or finite expansion of a multivariate function of interest. The general multivariate function response, $f(\mathbf{U})$ is expressed as the sum of contributions given by each parameter and their interactions, considered as increments with respect to a central value, f_c. Thus the A-cut HDMR decomposition can be given as:

$$f(\mathbf{U}) = f_c + \sum_{i=1}^{N_u} F_i(U_i) + \sum_{i<j<=N_u} F_{i,j}(U_i, U_j) + ... + F_{1,2,...,N_u}(U_1, U_2, ..., U_{N_u}), \tag{1}$$

where N_u is the number of parameters, F_i, $i = 1, \ldots, N_u$, are the orthogonal incremental contributions of every single parameter, $F_{i,j}$, $1 <= i < j <= N_u$, are the incremental contributions of each pair of parameters and $F_{1,2,...,N_u}$ is the incremental contribution of the interaction of all the parameters.

A surrogate model representation is independently generated for each incremental contribution and only for the non-zero elements, thus greatly reducing the complexity of sampling and building the model. Moreover, the contribution of each term of the sum to the global response is quantified independently so that higher-order interactions with low or zero contribution are neglected already by analysing the lower-order terms.

The A-cut-HDMR is adaptive in terms of sampling and truncation of terms in Equation (1). The existing input distribution and shape of the underlying response are considered for the adaptive sampling leading to an efficient distribution of samples for the given parameters and their combinations. The adaptive truncation removes any interactions that contribute less to the overall response than a prescribed threshold. Iteratively decreasing this threshold uncovers higher order interaction while keeping the number of required samples low.

2.2 Proper orthogonal decomposition-based data-driven reduced order modelling for aerodynamics

To ease the computational demands without sacrificing the quantitative accuracy of the study, the lower ranked interactions – for which many more points are sampled by the adaptive process – are obtained by in essence substituting CFD with an aerodynamic reduced order modelling (ROM). The data-driven ROM adopted here is based on POD [19]. Already available CFD solutions are collated into a snapshot set which is used to train the ROM. Then, within this work, the ROM database is used to obtain approximate surface solutions of the aerodynamic loads (in terms of pressure and shear stress) at any point in the parameter space, corresponding to particular operating conditions.

The POD-based ROM considered in this work is a popular non-intrusive model order reduction approach where the *method of snapshots* approach proposed by Sirovich [20] is coupled with radial basis function (RBF) interpolation. An approximate solution or *reconstruction* at any **x** location in the

parameter space, for the quantity of interest **u** can be obtained by a linear combination of the so-called POD modes or *basis functions*, so that:

$$\mathbf{u}(\mathbf{x}) \approx \hat{\mathbf{u}} = \sum_{i=1}^{N_m} a_i \phi_i(\mathbf{x}) \tag{2}$$

where $\hat{\mathbf{u}}$ is the approximation, ϕ_i denotes a POD mode, and a_i is the associated coefficient, which are summed over N_m modes. The POD modes are computed a-priori when generating the ROM database, while the coefficients are obtained using the RBF interpolation, an approach similar to that presented by Bui-Tanh et al. [21].

The POD algorithm itself is an approach that seeks the optimal linear subspace representation of the high-order data or *solution manifold*. The decomposition is optimal in the sense that the error between the truncated representation and the training data is minimised under the L^2 norm [19]. The *method of snapshots* approach shows that the POD modes can be expressed as linear combination of the high-order data, i.e. the CFD snapshot set. Then the modes can be expressed by solving an eigenvalue problem for the cross-correlation matrix of the snapshots. Operating on the cross-correlation matrix provides an advantage over the classical POD algorithm by significantly reducing the computational complexity of the low order model.

3.0 Definition of aerodynamic test case

The specific ultra-high aspect ratio strut-braced wing configuration – hereafter referred to only as SBW – considered in this study has been designed by ONERA and is intended to be equivalent to the Airbus A321neo which is a typical commercial mid-range aircraft. It has an aspect ratio $AR = 19$, and the geometry, specifically the wing and the strut are aerodynamically optimised for the design cruise conditions. A supercritical airfoil is employed on the wing, while a symmetric aerofoil is used for the strut. The optimised design of ONERA is based on the configuration presented by Méheut et al. [22].

The aircraft half-body geometry is initially meshed using an unstructured approach [23], before an appropriate boundary layer mesh is inserted using an advancing normal method [24].

This RANS-ready mesh is considered the baseline grid. For every study featured in this paper a separate anisotropic mesh adaptation step is performed in an iterative manner [24]. Multiple solutions – at various operating conditions – are combined for the adaptation metric, which addresses the possibly significant changes in the flow field across a given parameter space. The adaptation metric is Mach number and the level of grid convergence is assessed in terms of the variation of aerodynamic coefficients or angle-of-attack (AoA) depending on whether the study is fixed AoA or fixed C_L respectively. This mesh adaptation strategy allows for better refinement in critical regions of the flow, primarily capturing the wake and shock waves more accurately, while avoiding the need to perform additional mesh adaptation campaigns for each queried point in the parameter space, enabling also the use of the ROM approach. Initially, a reference grid converged mesh is created by combining solutions at a range of target C_L and design freestream conditions. This reference mesh is used for verification of the subsequent adaptation campaigns. Three levels of adaptation are performed until the mesh is considered grid converged, in the sense that the AoA and C_D at which all target C_L are achieved does not change between subsequent adaptation steps. Information on the baseline grid as well as a three-levels adapted mesh is presented in Table 1. A visualisation of the SBW configuration and adapted mesh is shown in Fig. 1.

Table 1. *Information on baseline grid and a three-levels adapted grid*

Mesh Adaptation	Number of Points	Number of Cells
Baseline	20,691,073	46,367,008
Three-levels adapted[a]	23,270,428	61,847,475

[a]Adapted grids generated for the subsequent sensitivity studies are coarser than the three-levels adapted mesh which is the finest grid.
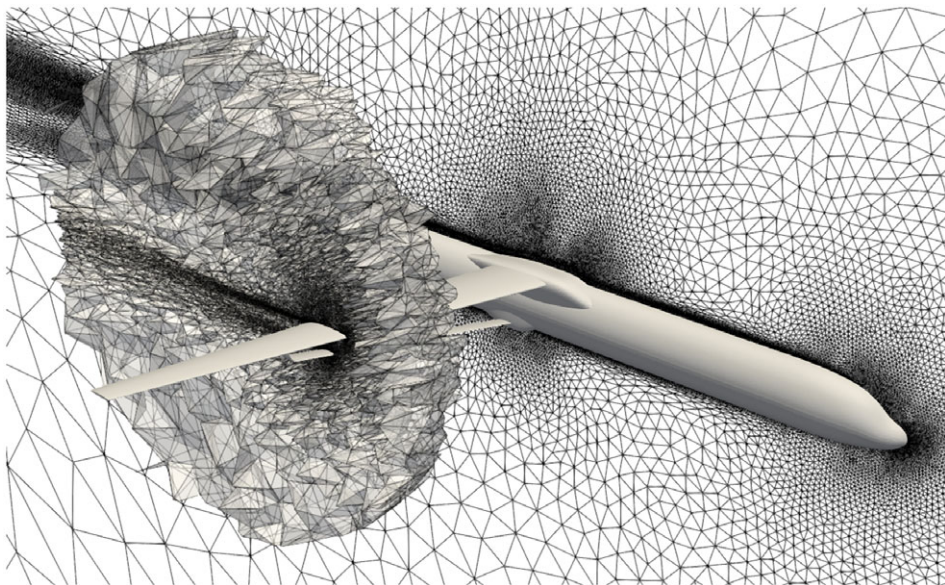
Figure 1. *Visualisation of an adapted mesh, after three iterations.*

Table 2. *Freestream quantities at the nominal point and cruise AoA*

Mach Number	Altitude (m)	Re/m	Angle-of-Attack (°)
0.75	12, 192	4.69×10^6	1.535

A consistent numerical setup was used for the RANS simulations. A finite volume discretisation of the fully turbulent Navier-Stokes is considered: the fluxes are discretised using the second-order Jameson-Schmidt-Turkel (JST) scheme [25], while turbulence is modeled using the Spalart-Allmaras (SA) model and is solved to first-order with a scalar upwind scheme. As per the boundary conditions for the body and the domain borders, adiabatic wall and far-field are considered respectively. The CFD module of the open-source code SU2 [26] was used for all computations. The freestream quantities at the nominal (cruise) point are listed in Table 2.

The surface solution at the nominal point is shown in Fig. 2. The critical areas of the geometry, specifically the wing-strut junction and the root of the strut are highlighted. Due to the complex geometry there is significant acceleration in the flow in those two areas, which leads to additional transonic shocks and potential side-of-body separation at the root.

4.0 Sensitivity of strut-braced wing to operating conditions

The A-cut HDMR approach is used to decompose the overall function response of lift to three independent parameters describing operating conditions: *altitude*, *velocity* and *AoA*. While the decomposition is done for dimensional quantities of the aerodynamic forces, all results are presented in terms of aerodynamic coefficients, C_L and C_D. The interest in assessing the sensitivities is to understand the design robustness of the SBW near cruise conditions to changes in operating conditions that can be likely experienced by the aircraft in flight, e.g. due to gusts or other external factors. The parameter space is defined around a central point, which corresponds to the nominal values defined in Table 2; the bounds of the design space are presented in Table 3 and were chosen so that all solutions are steady across the parameter space.
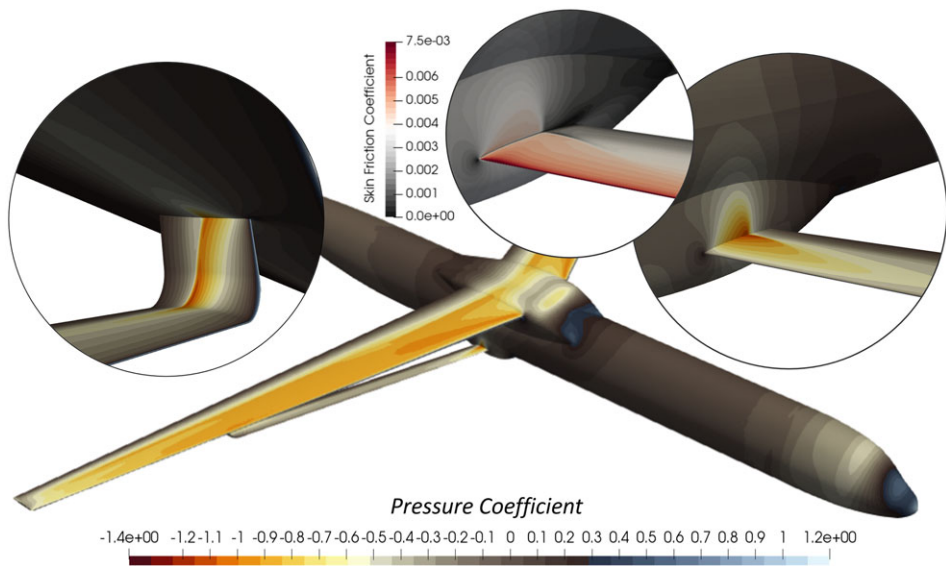
Figure 2. *CFD solution of the SBW in cruise. Pressure coefficient shows the overall flow on surface, including the shock along the wing, the wing-strut junction and at the root of the strut. The skin friction coefficient indicates some separation at the root.*

Table 3. *Parameter space of the sensitivity study*

Altitude (m)	Velocity (m/s)	Angle-of-attack (°)
$12,192 \pm 500$	221.3 ± 5.0	1.535 ± 0.50

In total, 43 CFD solutions were computed in the process, with the initial design of experiments accounting for 15 solutions. The average computational cost of one CFD simulation was 4,000 core hours, run on 252 to 360 CPU cores on an HPC cluster. The adaptive sampling was stopped once the total variance of the full surrogate reached a user-defined threshold. Since not all lower ranked contributions (increment functions) were uncovered by the purely high-fidelity approach – and it would be significantly more computationally expensive to sample a sufficient number of points for evaluating all increment functions – a dd-ROM is created from the existing solutions which then allows for fast approximation of the aerodynamic coefficients for points queried by the adaptive process. This ROM database can be generated within 1 hour on 1 core and predictions of new points are computed within minutes. The ROM reconstructions are surface solutions of the aerodynamic loads, pressure and skin friction coefficient. The forces are then integrated over the surface to obtain aerodynamic coefficients. The validation of the ROM is reported in Appendix A and was done via leave-one-out cross-validation as well as a comparison of HDMR surrogates obtained with the two approaches. Detailed tables of the responses of the aerodynamic coefficients are reported in Appendix B.

4.1 Sensitivity on lift coefficient

The domain decomposition for the lift was done using only CFD (HiFi approach) for all 1-factor and 2-factor contributions, while the ROM approach was used to obtain the 3-factor interaction. The 1-factor responses are shown in Fig. 3, presenting the incremental contributions and are all exhibiting a fairly linear response. Considering the whole domain a total of $\sum \Delta C_L = 0.3599$ can be achieved by varying the operating conditions, which is approximately 56% of the nominal value, $C_{L,cruise} = 0.638$.
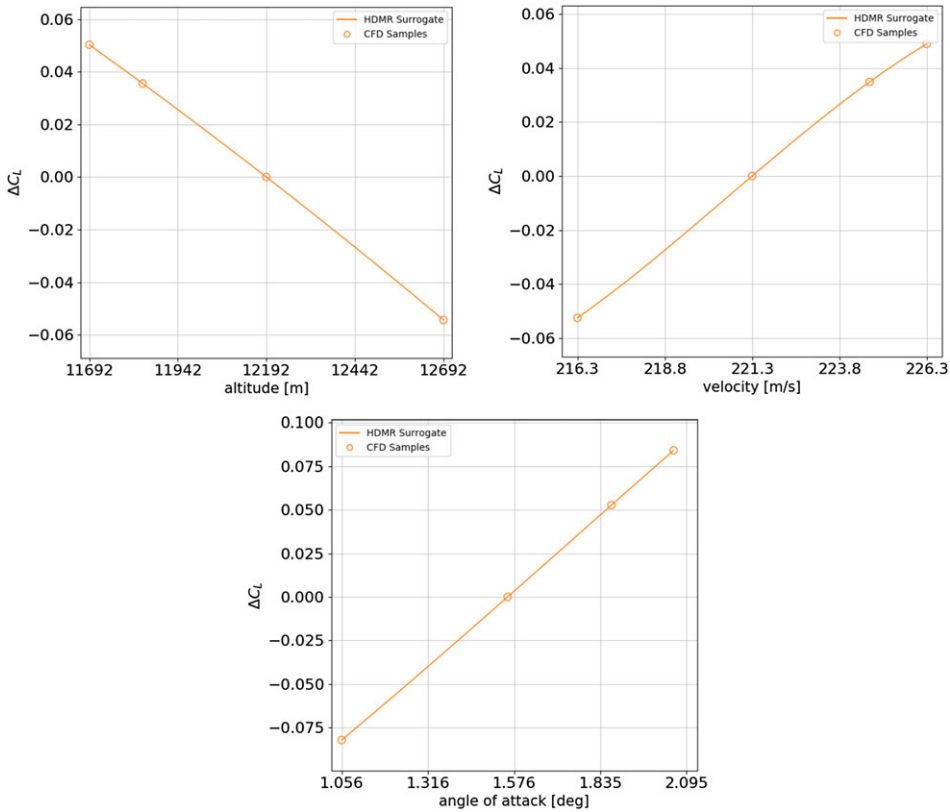
Figure 3. *1-factor contributions of altitude (left), velocity (right) and angle-of-attack (bottom) to C_L.*

The strongest parameter contributions are AoA and altitude. Thus, flying at the nominal velocity but at the lowest altitude and highest AoA the lift can be improved, while avoiding a much stronger shock wave on the wing. The surface solution is shown in Fig. 4, which also demonstrates the difference in shock wave intensity when compared with Fig. 2. With respect to cruise, the shock is stronger along the wing with a more pronounced lambda-shock-like feature near the root. However, the shock intensity near the root is largely unchanged, while the intensity decreases at the wing-strut junction.

4.2 Sensitivity on drag coefficient

The domain decomposition for the drag was done with the HiFi approach for all 1-factor and the most important 2-factor contributions, while the ROM approach was used to obtain the rest of the interactions.

The sensitivity of C_D is quite different to that of C_L. Velocity is the most important parameter, followed by AoA and finally altitude. Furthermore the incremental contribution of the interaction of velocity and AoA is of a similar magnitude to the individual parameter contributions. The 1-factor contributions are shown in Fig. 5. The response is linear only in the case of altitude and shows the most non-linearity in the case of velocity. This behaviour can be associated with transonic drag rise, brought on by the onset of drag divergence, however where exactly that occurs must be investigated in more detail. Nevertheless, increasing the cruise velocity leads to rapid increase in drag, indeed when considering the complete domain, approximately two-thirds of the range comes from increases in drag. Overall approximately 65% variation is experienced by the aircraft, with $\sum \Delta C_D = 156.56$ drag counts and the nominal value, $C_{D,cruise} = 239$ drag counts.
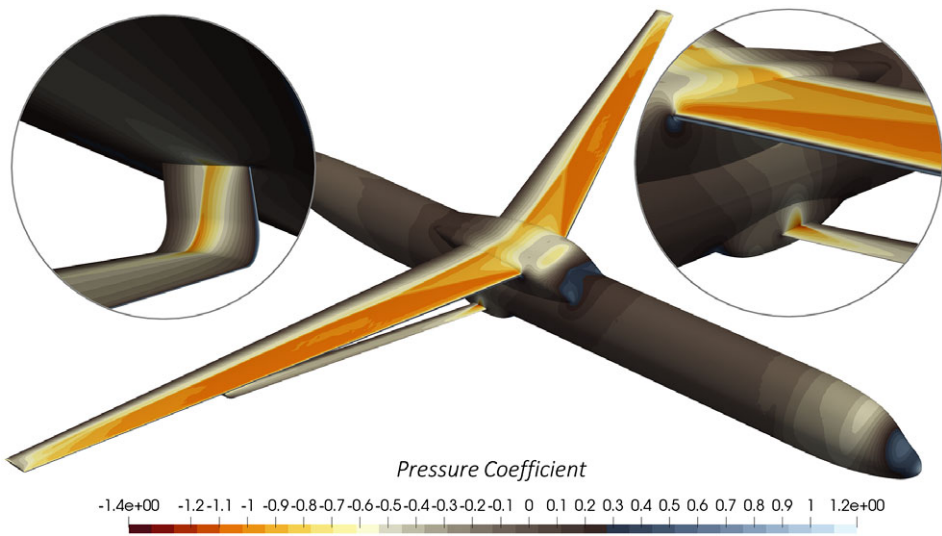
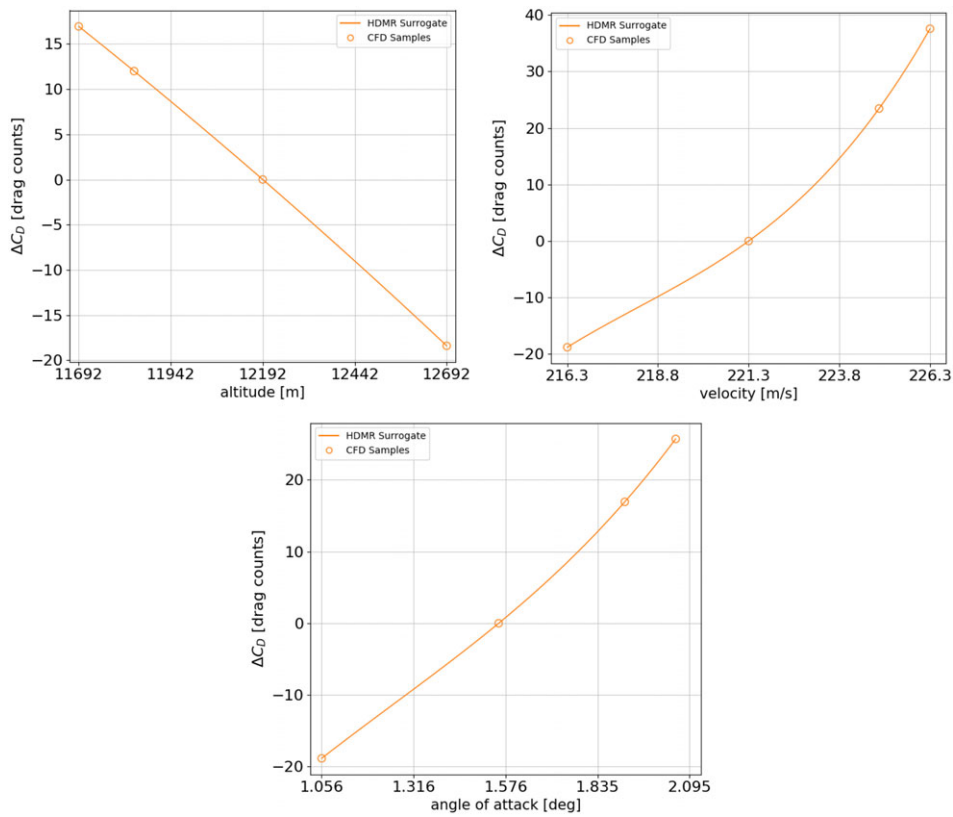**Figure 4.** *Pressure coefficient on the SBW surface for maximum C_L case.*

Figure 5. *1-factor contributions of altitude (left), velocity (right) and angle-of-attack (bottom) to C_D.*
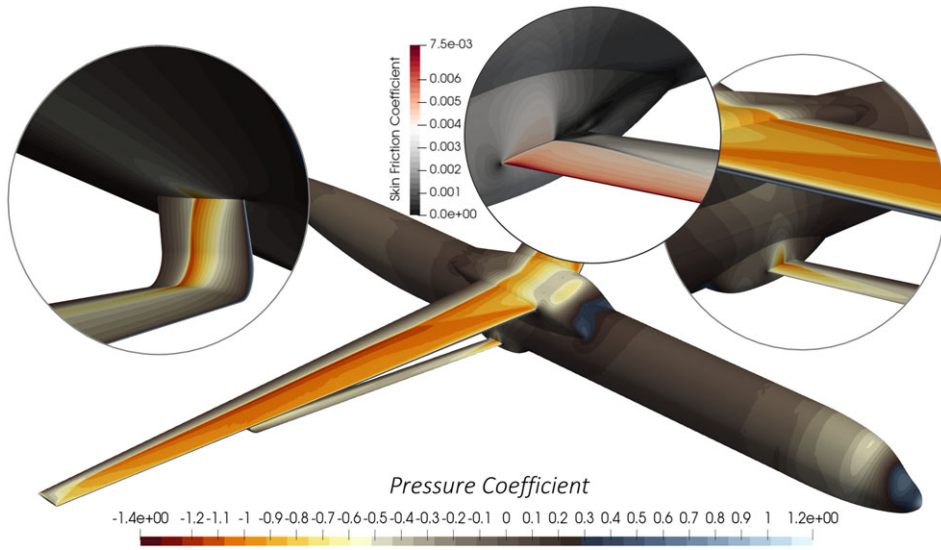
Figure 6. *CFD solution of the SBW at maximum C_D. With respect to cruise a significantly more intense shock is experienced along almost the whole span of the wing and at the wing-strut junction. There is also a substantial level of separation near the root of the strut as shown by the skin friction coefficient.*

As velocity and angle-of-attack increase the shock on the wing becomes much stronger. Similarly, the shock intensity at the root of the strut and near the attachment on the strut becomes stronger. Velocity especially also influences the spanwise extension of the two shocks on the strut, overall increasing wave drag. These effects are shown in Fig. 6.

4.3 Sensitivity on lift-to-drag ratio

The sensitivities for L/D are obtained by dividing the existing surrogates of lift and drag so that a more direct measure of the aircraft performance is obtained. To compute all contributions a combination of HiFi and ROM approach were used similarly to the lift and drag cases.

From Fig. 7 it follows that significant improvement of the aerodynamic performance cannot be achieved with respect to the design point. Sampling the maximum point of Fig. 8 and decreasing the flight altitude to the lower bounds an approximately 4.5% increase in L/D is observed. Corresponding to this maximum L/D case, Fig. 9 shows the surface pressure field on the aircraft with $L/D = 27.86$. In contrast to the maximum C_L case (e.g. Fig. 4), a slight reduction of cruise velocity leads to weaker shocks in all the critical regions of the flow, thus avoiding an increase in drag.

5.0 Comparative analysis with cantilever wing configuration

In an effort to quantify the influence of the strut on the overall sensitivity of the aircraft, the cantilever wing (CW) configuration is analysed with the same approach used for the SBW. Since the two configurations are otherwise identical any changes in the trends observed in the sensitivity analyses of Section 4 will be attributed to the absence of the strut. A comparison of the SBW and CW geometries as well as their adapted meshes is shown in Fig. 10.

To stay consistent the cruise C_L is not adjusted to account for the removal of the strut, as a structural model with appropriate weights is not considered in this study. The total reduction in C_D due to the absence of the strut is 18 drag counts. Note that the wing generates more lift in the case of the CW
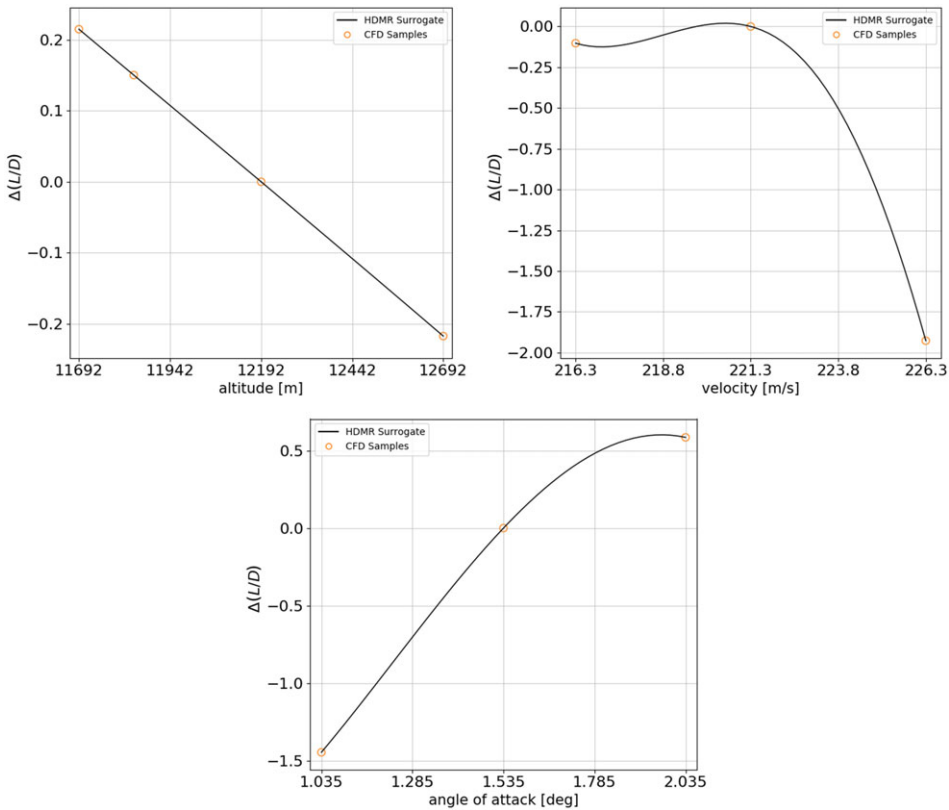
Figure 7. *1-factor contributions of altitude (left), velocity (right) and angle-of-attack (bottom) to L/D.*
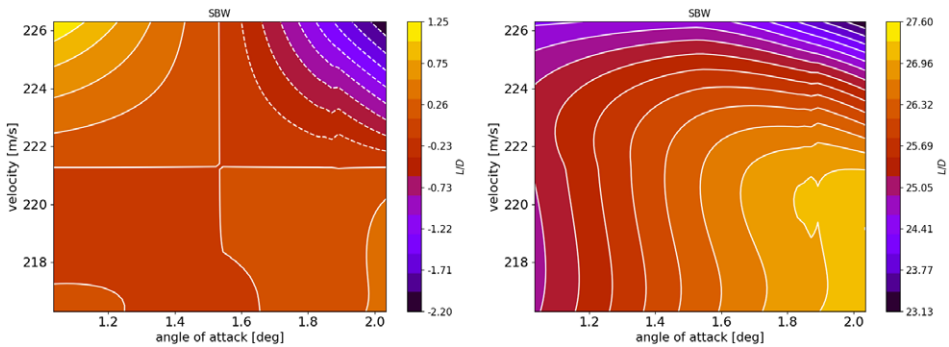

Figure 8. *Two-factor interaction (left) and combined contribution (right) of velocity and angle-of-attack to L/D.*

configuration as it flies at an approximately 0.1° higher AoA to offset the absence of the strut which provides about 5% of the total lift.

Figure 11 shows the comparison of 1-factor function responses. From this it follows that removing the strut does not affect the design robustness around cruise as the differences between CW and SBW are very small. Quantitatively the difference in total range within the parameter space is only 1.4 drag counts.
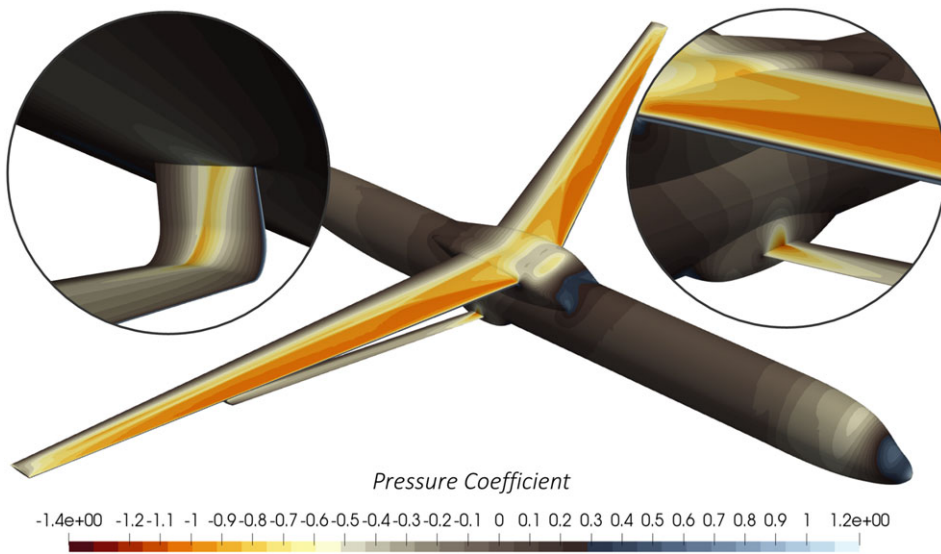
Figure 9. *Pressure coefficient on the SBW surface for maximum L/D case. A weaker shock is observed at the wing-strut junction which contributes to reduced drag and improved performance.*
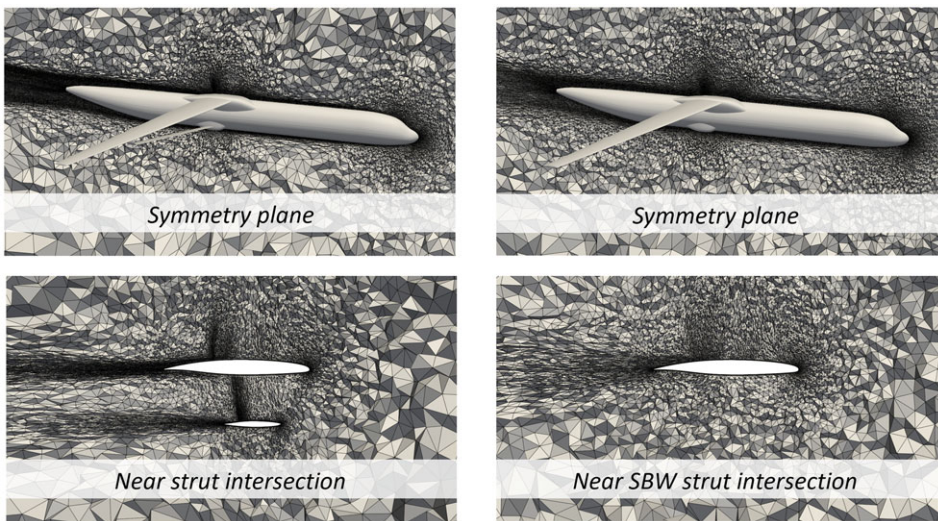

Figure 10. *Adapted mesh of the SBW (left) and CW (right) at symmetry plane and near strut intersection.*

Comparing aerodynamic loads on the wing reveals further insights, supporting the results of the sensitivity analysis. Figure 12 shows a comparison of the pressure coefficient. The flow on the pressure side of the wing is influenced significantly by the strut due to the nozzle effect but only near the wing-strut junction. The effect outboard of the junction is negligible. Inboard of the strut at mid-chord the pressure is slightly lower when the strut is present, noting also the presence of a small transonic shock feature as the flow accelerates near the junction of the SBW. On the suction side much of the same flow features are present in the two cases, although on the inboard section the flow appears to accelerate more
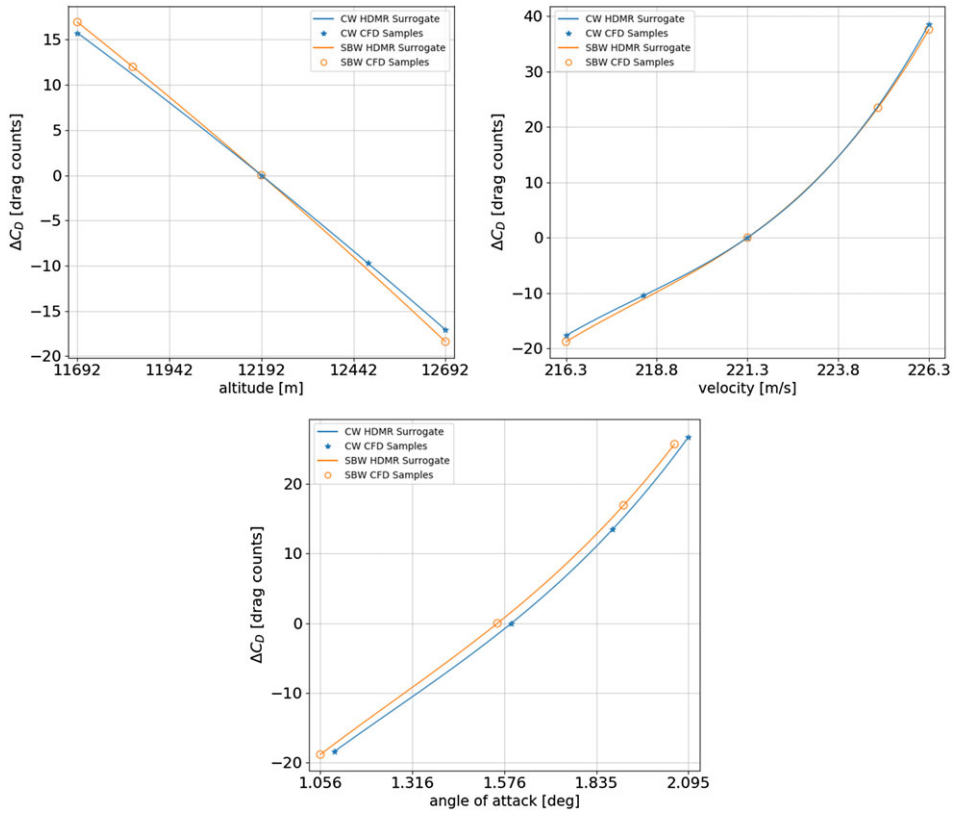
Figure 11. *One-factor contributions of altitude (left), velocity (right) and angle-of-attack (bottom) to C_D for the cantilever wing configuration.*
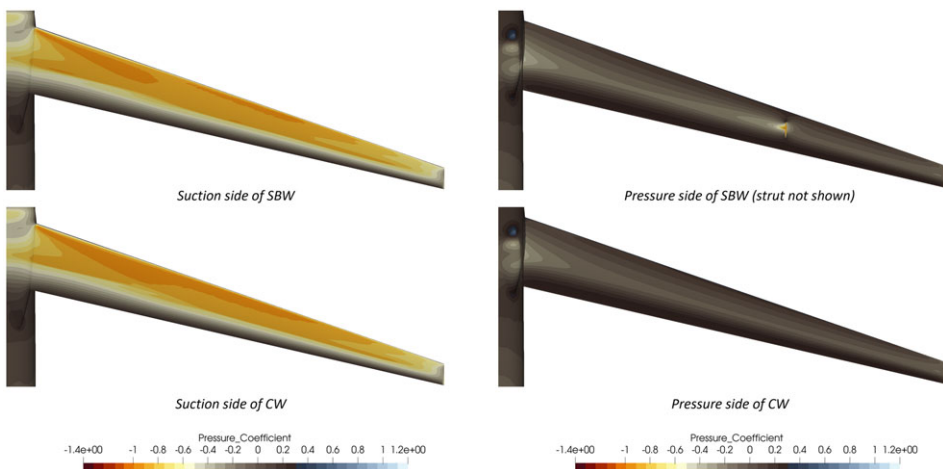

Figure 12. *Comparison of pressure coefficient on the SBW and CW wing for cruise (strut not shown).*
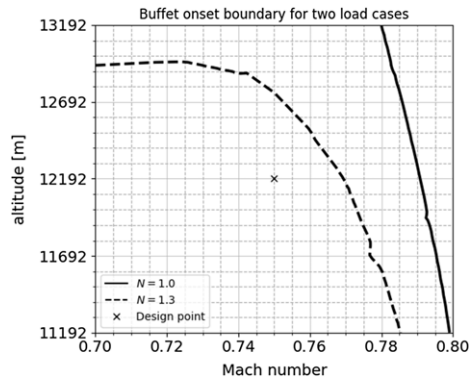
Figure 13. *Buffet limits at N = 1.0 and N = 1.3. Boundary defined at buffet onset corresponding to 6% separation on the wing.*

on the CW configuration, attributed to a combination of marginally higher angle-of-attack, differences in the grid and potentially affected by the absence of the strut.

6.0 Identification of buffet limits through an exploration of operating conditions

While the previous analyses assessed the impact of varying operating conditions on the aerodynamic behaviour, the wider exploration instead aims to characterise transonic effects at fixed load factors and varying freestream parameters. The load factors considered are $N = 1.0$ and $N = 1.3$, with corresponding flight conditions of steady level cruise and an approximately 40° banking turn (or moderate turbulence) respectively. Moreover, the load factor $N = 1.3$ is commonly specified as the safety margin at which the aircraft must remain buffet free. Thus it is important to ensure that the SBW design fulfills these requirements. Assessing the transonic drag rise due to changing freestream conditions allows for further insights e.g. in terms of drag divergence, a behaviour which was indicated already from the results presented in Subsection 4.3.

Transonic buffet is an unsteady flow phenomenon arising from shock wave – boundary layer interaction, specifically shock induced flow separation. While the physics is not fully understood, the separation is associated with a self-sustained shock oscillation. This oscillation is not only undesirable in terms of aerodynamics but can induce a detrimental structural response, hence the aforementioned safety margin, i.e. a limit on the aircraft's flight envelope. The onset of buffet is ambiguously defined and there are various criteria predicting it from several steady solutions or by computing unsteady simulations [27]. As the study done here aims to identify buffet onset across the whole parameter space, requiring many simulations, the approach introduced by Kenway and Martins [28] is adopted. They predict buffet onset from a single steady-state solution by evaluating the amount of flow separation, by considering the sign of the streamwise component of skin friction. Their approach is verified against the standard $\Delta \alpha = 0.1$ method [27, 29]. The amount of backflow corresponding to buffet onset is found via this verification (see Appendix C) and is identified as $\sigma = 6.013\%$. This value is then used as the buffet onset criterion throughout the parameter space.

RANS and time-averaged unsteady RANS simulations were used to identify buffet onset and evaluate drag rise across the parameter space. Figure 13 shows the buffet limits, highlighting that for $N = 1.0$ significant changes in operating conditions are acceptable and the cruise C_L can be achieved throughout much of the parameter space. In the case of $N = 1.3$ buffet onset is observed at approximately $M = 0.77$ at cruise altitude, indicating that at the design point the safety margins are respected. Increasing cruise altitude however is severely limiting, the aircraft cannot safely fly above 12.942km, the altitude which
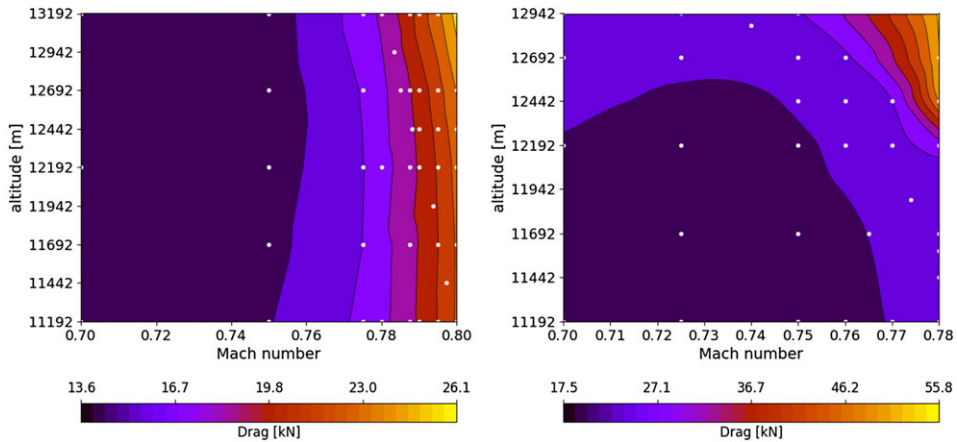
Figure 14. *Drag rise at N = 1.0 (left) and N = 1.3 (right). White dots mark the CFD solutions used for the plots. Dimensional quantities shown to aid interpretation of the figures.*
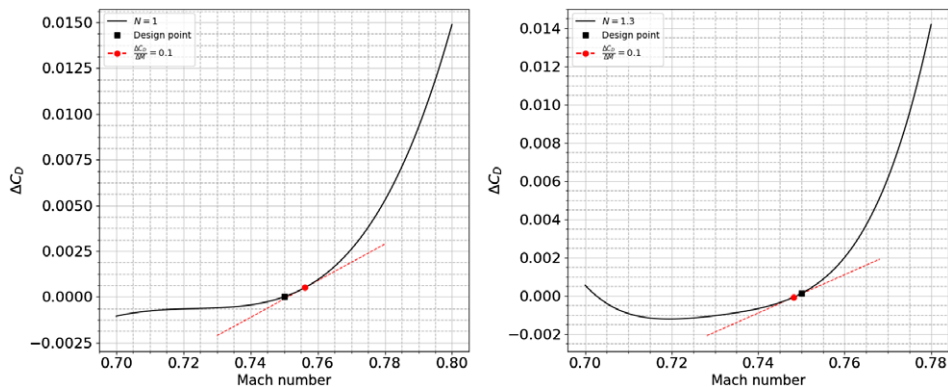

Figure 15. *Drag divergence at N = 1.0 (left) and N = 1.3 (right) at cruise altitude.*

corresponds to the *buffet ceiling*. This behaviour is attributed to the rapid increase of required AoA at the lower Mach and increased altitude. Note here however that since the configuration is optimised for maximum cruise performance it was not designed with a buffet constraint in mind.

The drag rise for both load cases is shown in Fig. 14, The effects of drag divergence are clearly observed for load factor $N = 1.0$, exhibiting similar trends to that seen in the sensitivity analysis. While the buffet margin is sufficiently far from the cruise Mach and is not limited by altitude (within the bounds of the parameter space), the rapid increase in drag for a given target lift makes increases in Mach number undesirable.

Indeed, as shown in Fig. 15, the drag divergence Mach number at the cruise altitude is $M = 0.7562$, which is not far above the cruise Mach; while in the case of $N = 1.3$ drag divergence is already observed at the cruise Mach number. Note that the drag divergence was assessed for constant lift and the criterion of $\Delta C_D/\Delta M = 0.1$ [30]. For the load case $N = 1.3$ the upper bounds of the parameter space are restricted due to significant unsteadiness in some regions: the maximum altitude is only 12,942m and the maximum Mach number is 0.78. At the lower altitudes the drag increases as expected: at the lower Mach numbers drag is lowest and with increases in Mach the rate of the drag rise becomes faster. However,

around cruise altitude and above, the drag minima are observed not at the lowest Mach number, with the behaviour shown also in Fig. 14. This effect is again attributed to flying at comparatively much higher AoA, which in turn means a faster rate of increase in drag.

7.0 Concluding remarks

Within this work, the aerodynamic behaviour of a given mid-range UHAR-SBW airframe is explored near cruise conditions. This is achieved by a study of the sensitivity of lift and drag as well as lift-to-drag ratio to three parameters describing operating conditions. The influence of the strut on the sensitivities is quantified by way of comparison with a cantilever wing configuration. To gain further insights, specifically into transonic effects, an additional analysis is made that characterises drag rise and drag divergence at fixed load factors. Moreover, the boundary of buffet onset is identified across the parameter space. The importance of this is highlighted as buffeting poses a limit to an aircraft's flight envelope in terms of cruise Mach number and altitude.

When considering lift, the response of sensitivities to individual parameters is largely linear and AoA has the largest influence. To improve C_L, decreasing altitude has a similar magnitude but slightly larger effect than increasing cruise velocity, while avoiding more intense shock waves. In the case of drag the most important parameter is velocity, whose response is non-linear, leading to rapid increase of C_D above the central value. It is shown that this is due to drag divergence; the increase in wave drag can be inferred from the severity of shock waves when comparing the case of maximum drag with that of cruise. In terms of drag reduction, when considering individual parameters their influence is of very similar magnitude. Ultimately, however, the metric for performance is L/D. Within the parameter space only a marginal improvement can be achieved with respect to the central point. Indeed, flying any higher than the design cruise velocity is detrimental to performance. Again, this is attributed to the onset of drag divergence. It is is worth noting that this configuration was specifically designed so that in cruise the aerodynamic performance is maximised, explaining why significant transonic effects suddenly appear when increasing velocity or AoA. Within the framework of the Clean Aviation programme ONERA is currently working on another SBW configuration with the aim of improved performance at higher cruise Mach numbers and lift coefficients.

Regarding the comparison with the CW configuration, it is clear that for SBW designs it is possible for the strut to have little influence on robustness of the design near cruise conditions, provided there is heavy emphasis on the aerodynamic optimisation of the strut. For the configuration assessed in this work the interference effects are minimal and have little extension beyond the region of the wing-strut junction. Another advantage of the optimised strut is that there is no shock wave extending across its span, instead the two shock waves are localised only near the root and near the junction, due to the channeling effect further accelerating the flow. Therefore, the wave drag of the strut is kept low. Note however that the strut is primarily a structural component so coupled aero-structural optimisation is critical; which may lead to less aerodynamically efficient (e.g. thicker) strut designs. Nevertheless, these results are promising for the viability of the SBW concept: as long as the aeroelastic and structural behaviour is acceptable, the aircraft can not only outperform modern conventional configurations, but its predicted gains in L/D approach the optimistic estimates quoted in literature.

Finally, a wider exploration of the operating conditions at fixed load factors revealed that while the aircraft satisfies requirements in terms of buffeting, its design point is not very far removed from the boundary of the flight envelope (determined by the buffet onset). Steady level cruise can be achieved across much of the wider parameter space without an indication of buffet onset. An analysis of the drag rise shows rapid increase at Mach number beyond the design value, similarly to the results of the sensitivity analysis. The implications of all the analyses is that a slightly reduced cruise Mach number as well as flying at a lower altitude can lead to marginal gains in performance, and more importantly allow the aircraft to fly further away from the upper bounds of its flight envelope, with the additional benefit of more robustness to changes in operating conditions.

Competing interests. The authors declare none.

References

[1] Abbas, A., de Vicente, J. and Valero, E. Aerodynamic technologies to improve aircraft performance, *Aerospace Sci. Technol.*, 2013, **28**, (1), pp 100–132, doi: 10.1016/j.ast.2012.10.008

[2] Chau, T. and Zingg, D. Aerodynamic optimization of a transonic strut-braced-wing regional aircraft based on the reynolds-averaged Navier-Stokes equations, AIAA AVIATION 2021 FORUM, Virtual Event, July 2021, doi: 10.2514/6.2021-2526

[3] Zhu, M., Li, Y., Qin, N., Huang, Y., Deng, F., Wang, Y. and Zhao, N. shock control of a low-sweep transonic laminar flow wing, *AIAA J.*, 2019, **57**, (6), pp 2408–2420, doi: 10.2514/1.J058011

[4] Bradley, M.K., Droney, C.K. and Allen, T.J. Subsonic Ultra Green Aircraft Research: Phase II – Volume I – Truss Braced Wing Design Exploration, NASA, 2015.

[5] Carrier, G., Atinault, O., Dequand, S., Hantrais-Gervois, J.-L., Liauzun, C. and Paluch, B. Investigation Of A strut-braced wing configuration for future commercial transports, 28th Congress of the International Council of the Aeronautical Sciences 2012, ICAS, January 2012.

[6] Chau, T. and Zingg, D.W. Aerodynamic design optimization of a transonic strut-braced-wing regional aircraft, *J. Aircraft*, 2022, **59**, (1), pp 253–271, doi: 10.2514/1.C036389

[7] Ko, A., Mason, W. and Grossman, B. Transonic aerodynamics of a wing/pylon/strut juncture, 21st AIAA Applied Aerodynamics Conference, June 2003, doi: 10.2514/6.2003-4062

[8] Ma, Y., Karpuk, S. and Elham, A. Conceptual design and comparative study of strut-braced wing and twin-fuselage aircraft configurations with ultra-high aspect ratio wings, *Aerospace Sci. Technol.*, 2022, **121**, doi: 10.1016/j.ast.2022.107395

[9] Secco, N.R. and Martins, J.R.R.A. RANS-based aerodynamic shape optimization of a strut-braced wing with overset meshes, *J. Aircraft*, 2019, **56**, (1), pp 217–227, doi: 10.2514/1.C034934

[10] Gur, O., Bhatia, M., Schetz, J., Mason, W., Kapania, R. and Mavris, D. design optimization of a truss-braced-wing transonic transport aircraft, *J. Aircraft*, 2010, **47**, (1), pp 1907–1917, doi: 10.2514/1.47546

[11] Seber, G, Ran, H., Nam, T., Schetz, J. and Mavris, D. Multidisciplinary design optimization of a truss braced wing aircraft with upgraded aerodynamic analyses, 29th AIAA Applied Aerodynamics Conference, June 2011, doi: 10.2514/6.2011-3179

[12] Sohst, M., do Vale, J.L., Afonso, F. and Suleman, A. Optimization and comparison of strut-braced and high aspect ratio wing aircraft configurations including flutter analysis with geometric non-linearities, *Aerospace Science and Technology*, 2022, **124**, doi: 10.1016/j.ast.2022.107531

[13] Chakraborty, I., Nam, T., Gross, J.R., Mavris, D.N., Schetz, J.A. and Kapania, R.K. Comparative assessment of strut-braced and truss-braced wing configurations using multidisciplinary design optimization, *J. Aircraft*, 2015, **52**, (6), pp 2009–2020, doi: 10.2514/1.C033120

[14] Gong, C. and Ma, B.-F. Shape optimization and sensitivity analysis of a morphing-wing aircraft, *Int. J. Aeronaut. Space Sci.*, 2019, **20**, pp 57–69, doi: 10.1007/s42405-018-0110-7

[15] Jones, B., Nagy, P., Minisci, E. and Fossati, M. A geometric sensitivity study for the aerodynamics of a strut-braced airframe, *Aerospace Sci. Technol.*, 2023, **142**, doi: 10.1016/j.ast.2023.108638

[16] Kubicek, M., Minisci, E. and Cisternino, M. High dimensional sensitivity analysis using surrogate modeling and high dimensional model representation, *Int. J. Uncertainty Quantif.*, 2015, **5**, (3), doi: 10.1615/Int.J.Uncertainty Quantification.2015012033

[17] Kubicek, M. High dimensional uncertainty propagation for hypersonic flows and entry propagation, 2018, University of Strathclyde, doi: 10.48730/9dy2-st94

[18] Mehta, P.M., Kubicek, M., Minisci, E. and Vasile, M. Sensitivity analysis and probabilistic re-entry modeling for debris using high dimensional model representation based uncertainty treatment, *Adv. Space Res.*, 2015, **59**, (1), pp 193–211, doi: 10.1016/j.asr.2016.08.032

[19] Holmes, P., Lumley, J.L. and Berkooz, G. *Turbulence, Coherent Structures, Dynamical Systems and Symmetry*, Cambridge University Press, 1996, Cambridge, UK.

[20] Sirovich, L. Turbulence and the dynamics of coherent structures. I - Coherent structures. II - Symmetries and transformations. III - Dynamics and scaling, *Q. Appl. Math.*, 1987, **45**, doi: 10.1090/qam/910463

[21] Bui-Thanh, T. and Damodarany, M. Proper orthogonal decomposition extensions for parametric applications in transonic aerodynamics, 21st AIAA Applied Aerodynamics Conference, June 2003, doi: 10.2514/6.2003-4213

[22] Méheut, M., Arnoult, G., Atinault, O., Bennehard, Q. and François, C. Overview of aerodynamic design activities performed at ONERA to reduced aviation's climate impact, 33rd Congress of the International Council of the Aeronautical Sciences 2022, ICAS, September 2022.

[23] Geuzaine, C. and Remacle, J.-F. Gmsh: A 3-D finite element mesh generator with built-in pre- and post-processing facilities, *Int. J. Numer. Methods Eng.*, 2009, **79**, pp 1309–1331, doi: 10.1002/nme.2579

[24] Alauzet, F. and Frazza, L. Feature-based and goal-oriented anisotropic mesh adaptation for RANS applications in aeronautics and aerospace, *J. Comput. Phys.*, 2021, **439**, doi: 10.1016/j.jcp.2021.110340

[25] Jameson, A. Origins and further development of the Jameson–Schmidt–Turkel scheme, *AIAA J.*, 2017, **55**, (5), pp 1487–1510, doi: 10.2514/1.J055493

[26] Economon, T.D., Palacios, F., Copeland, S.R., Lukaczyk, T.W. and Alonso, J.J. SU2: An open-source suite for multiphysics simulation and design, *AIAA J.*, 2016, **54**, (3), doi: 10.2514/1.J053813

[27] Breitenstein, C. Overview of criteria to estimate aerodynamic limits of the flight envelope of a transonic aircraft based on RANS simulations, *CEAS Aeronaut. J.*, 2023, **14**, doi: 10.1007/s13272-023-00685-8

[28] Kenway, G. and Martins, J. Buffet-onset constraint formulation for aerodynamic shape optimization, *AIAA J.*, 2017, **55**, pp 1–18, doi: 10.2514/1.J055172

[29] Sartor, F. and Timme, S. Mach number effects on buffeting flow on a half wing-body configuration, 50th 3AF International Applied Aerodynamics Conference, Toulouse, France, March 2015.

[30] Roskam, J. and Lan, C.T.E. *Airplane Aerodynamics and Performance*, DARcorporation, 1997, Lawrence, KS, USA.

Appendix

A. Validation of aerodynamic reduced order model of strut-braced wing

Figure A1 shows the results of the leave-one-out cross-validation in terms of lift and drag. A direct comparison was made between lift and drag values obtained from the ROM reconstruction of surface solutions and the corresponding CFD solution. The maximum errors are below 4%. Figure A2 shows a good agreement between surrogates obtained via CFD and the ROM methodology, respectively. The verification for the cantilever ('clean') wing is also shown, although the ROM database is used only for the strut-braced wing (SBW) within this work.
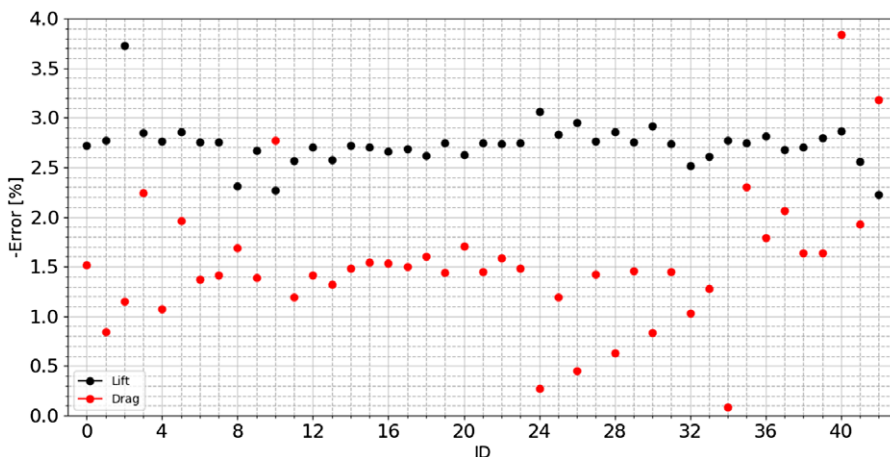

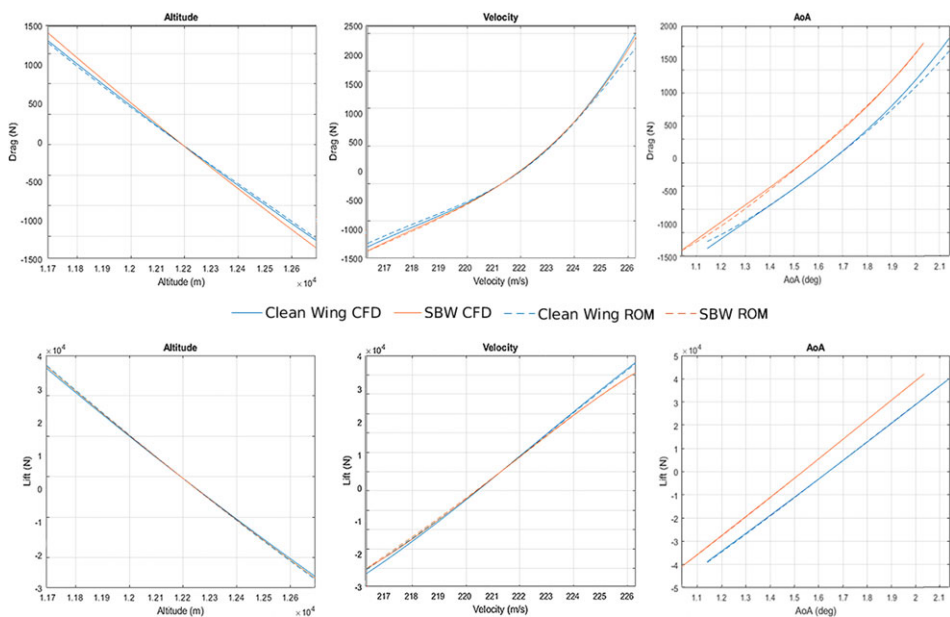***Figure A1.*** *Leave-one-out errors of the SBW dd-ROM.*

Figure A2. *Verification of the ROM approach. One-factor surrogates obtained from CFD and ROM are compared.*

B. Tables of sensitivities of the aerodynamic coefficients

Table B1 presents the sensitivities of L/D as well as the gradient of each parameter at the cruise point, which indicates the effect of small perturbations on the SBW. However, the global trends are not predicted well by the gradient when significant nonlinearity is observed across the parameter space.

Tables B2 and B3 show the detailed sensitivities of each parameter contribution and their interactions for C_L and C_D, respectively. In Table B4 the sensitivity of drag is presented for the CW configuration, with the ranges showing little deviation from Table B3. Note that the comparison of lower-ranked interactions is omitted. These could be only compared via the ROM approach, which have a higher inherent prediction error than the expected differences in the sensitivities. The net effect of all interactions is computed using an optimisation on the full surrogate to find the minimum and maximum and thus the total combined range.

Table B1. *Table of sensitivities for L/D*

Function	Min Δ (L/D)	Max Δ (L/D)	L/D Range	Combined	Gradient[a]
α	−5.422	2.255	7.678	7.678	9.32
v	−7.224	0.0738	7.298	7.298	−7.224
h	−0.8146	0.805	1.62	1.62	−0.0016
v - α	−8.26	4.672	12.93	16.75	–
h - α*	−0.419	0.383	0.802	9.098	–
h - v*	−0.7996	0.7407	1.54	8.318	–
h - v - α*	−0.8079	0.7574	1.565	19.09	–
All	−13.96	5.129	–	19.09	–

All quantities are in terms of percentages.
[a]Gradients are in terms of percentages over respective unit of the parameter.
*Marks results obtained using the ROM approach. Also shown are first-order gradients computed at the central point using finite difference.

Table B2. *Table of sensitivities for C_L*

Function	Min ΔC_L	Max ΔC_L	C_L Range	Combined
α	-0.082150	0.0841	0.1662	0.1662
h	-0.05432	0.05031	0.10465	0.1046
v	-0.05253	0.0489	0.1014	0.1014
h - α	-0.007141	0.006954	0.0141	0.2705
v - α	-0.009245	0.007904	0.01715	0.2559
h - v	-0.004317	0.004624	0.008941	0.2054
h - v - α^*	-0.000807	0.000862	0.001669	0.3599
All	-0.1702	0.1897	–	0.3599

*Marks results obtained using the ROM approach.

Table B3. *Table of sensitivities for C_D*

Function	Min ΔC_D	Max ΔC_D	C_D Range	Combined
v	-18.80	37.58	56.385	56.385
α	-18.84	25.71	44.55	44.55
h	-18.40	16.94	35.35	35.35
v - α	-11.91	19.03	30.95	117.2
h - v^*	-3.43	3.21	6.63	93.38
h - α^*	-2.31	2.16	4.47	80.44
h - v - α^*	-1.75	1.60	3.34	156.6
All	-50.36	106.20	–	156.6

All quantities are in terms of drag counts.
*Marks results obtained using the ROM approach.

Table B4. *Table of sensitivities for C_D for the cantilever wing configuration*

Function	Min ΔC_D	Max ΔC_D	C_D Range	Combined
v	-17.69	38.52	56.21	56.21
α	-18.42	26.73	45.15	45.15
h	-17.08	15.75	32.83	32.83
v - α	-13.69	19.73	33.42	118.2
All	-50.34	100.7	–	151.1

All quantities are in terms of drag counts.

C. Verification and assessment of buffet onset criterion

The Kenway and Martins method of identifying a buffet onset criterion from the amount of backflow is verified. This process is also used to update the value of the criterion σ, so it is specific for this aircraft configuration. The $\Delta\alpha = 0.1$ method is applied for the nominal operating conditions, with the results shown in Fig. C1. For these conditions buffet onset is predicted at $\alpha = 3.4°$ with the amount of backflow on the wing being $\sigma = 6.013\%$.
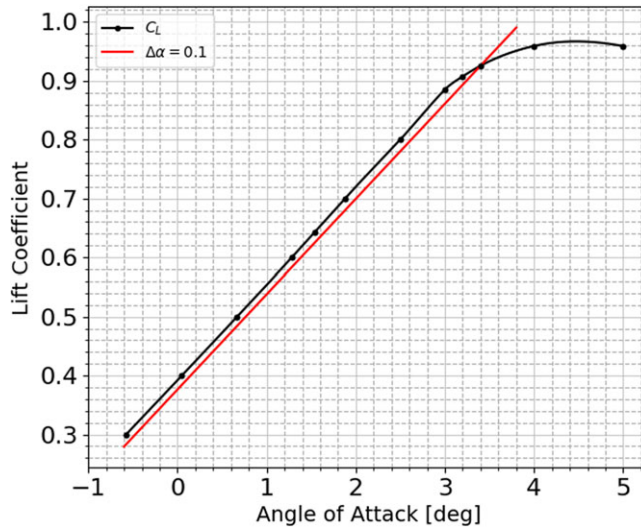
Figure C1. *Application of $\Delta\alpha = 0.1$ method at cruise condition to identify buffet onset.*